JACS
JOURNAL OF THE AMERICAN CHEMICAL SOCIETY

Article

pubs.acs.org/JACS

Influence of Anion Delocalization on Electron Transfer in a Covalent Porphyrin Donor–Perylenediimide Dimer Acceptor System

Patrick E. Hartnett, Catherine M. Mauck, Michelle A. Harris, Ryan M. Young, Yi-Lin Wu, Tobin J. Marks,* and Michael R. Wasielewski*

Department of Chemistry and Argonne-Northwestern Solar Energy Research (ANSER) Center, Northwestern University, 2145 Sheridan Road, Evanston, Illinois 60208, United States

Supporting Information

ABSTRACT: Photodriven electron transfer from a donor excited state to an assembly of electronically coupled acceptors has been proposed to enhance charge transfer efficiency in functional organic electronic materials. However, the circumstances under which this may occur are difficult to investigate in a controlled manner in disordered donor–acceptor materials. Here we investigate the effects of anion delocalization on electron transfer using zinc *meso*-tetraphenylporphyrin (ZnTPP) as a donor and a perylene-3,4:9,10-bis(dicarboximide) dimer as the acceptor (PDI_2). The PDI units of the dimer are positioned in a cofacial orientation relative to one another by attachment of the imide group of each PDI to the 4- and 5-positions of a xanthene spacer. Furthermore, the distal imide group of one PDI is linked to the *para*-position of one ZnTPP phenyl group to yield ZnTPP-PDI_2. The data for the dimer are compared to two different ZnTPP-PDI monomer reference systems designed to probe electron transfer to each of the individual PDI molecules comprising PDI_2. The electron transfer rate from the ZnTPP lowest excited singlet state to PDI_2 is increased by 50% relative to that in ZnTPP-PDI, when the data are corrected for the statistics of having two electron acceptors. Femtosecond transient IR absorption spectroscopy provides evidence that the observed enhancement in charge separation results from electron transfer producing a delocalized PDI_2 anion.

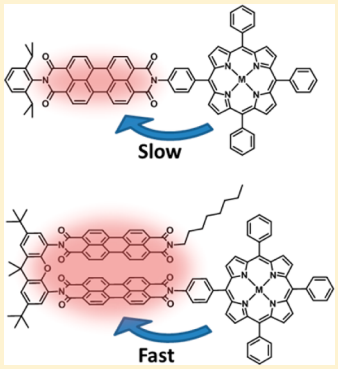

INTRODUCTION

Photoinduced charge separation is ubiquitous in organic materials ranging from models for photosynthetic reaction center proteins[1−5] to organic photovoltaics (OPVs).[6−10] If two or more electron acceptors are strongly electronically coupled, electron transfer may occur from a donor molecule to a molecular orbital delocalized over the acceptors. Moreover, if electron transfer occurs on a subpicosecond time scale, this process may also be electronically coherent.[11−13] Recently, it has been proposed that the electronic interaction of two or more electron acceptors can result in enhanced electron transfer rates and efficiencies that could favorably enhance charge generation and transport within functional organic materials.[7−10,14,15]

One important example of this general problem has arisen in the field of organic photovoltaics (OPVs), many of which undergo exciton dissociation in <100 fs.[16−19] As the charge transfer step is integral to overall power conversion efficiency (PCE),[20] this phenomenon has been the subject of extensive theoretical and experimental investigations.[7−10] This rapid process is not limited to charge separation at the donor–acceptor interface, but can be attributed to the dissociation of delocalized excitons centered several nanometers from the interface and can result in free charge carriers with an initial electron–hole pair separation of at least 4 nm within 40 fs of excitation.[7,21] The mechanism of free carrier formation is a subject of current debate and conflicts with the Onsager-Braun model of charge carrier dissociation, which predicts the formation of Coulombically trapped electron–hole pairs at the donor–acceptor interface.[22,23] The observed ultrafast rates and high yields of charge separation in OPVs have been associated with either the dissociation of a "hot" charge-transfer state prior to vibrational cooling,[24−26] or by charge transfer directly into a delocalized state of a fullerene cluster.[8,9,21,27−29]

In many cases, the high yield of free carriers in OPVs has been attributed to the ability of fullerene acceptors to electronically couple to donor molecules in three dimensions, which leads to improved entropic gains upon charge separation,[30] increased delocalization of radical anions,[8] increased initial separation of the photoinduced radical ion pair,[31] and improved charge transport upon dissociation.[32] As a consequence of this reasoning, the vast majority of high-efficiency OPVs have used a fullerene derivative as the electron acceptor.[33−35] However, fullerenes are expensive, difficult to modify, and absorb light poorly, which has led to a recent surge of interest in developing small molecule and polymer-based acceptors to replace fullerenes.

Some of the most successful nonfullerene acceptors are perylene-3,4:9,10-bis(dicarboximide) (PDI) derivatives, which have provided PCEs in OPVs over 9%.[36] Most of these efficient OPV's capitalize on twisted covalent PDI dimers or oligomers

Received: September 28, 2016
Published: December 27, 2016

DOI: 10.1021/jacs.6b10140
J. Am. Chem. Soc. 2017, 139, 749−756

Scheme 1. Structures of Molecules Used in This Study

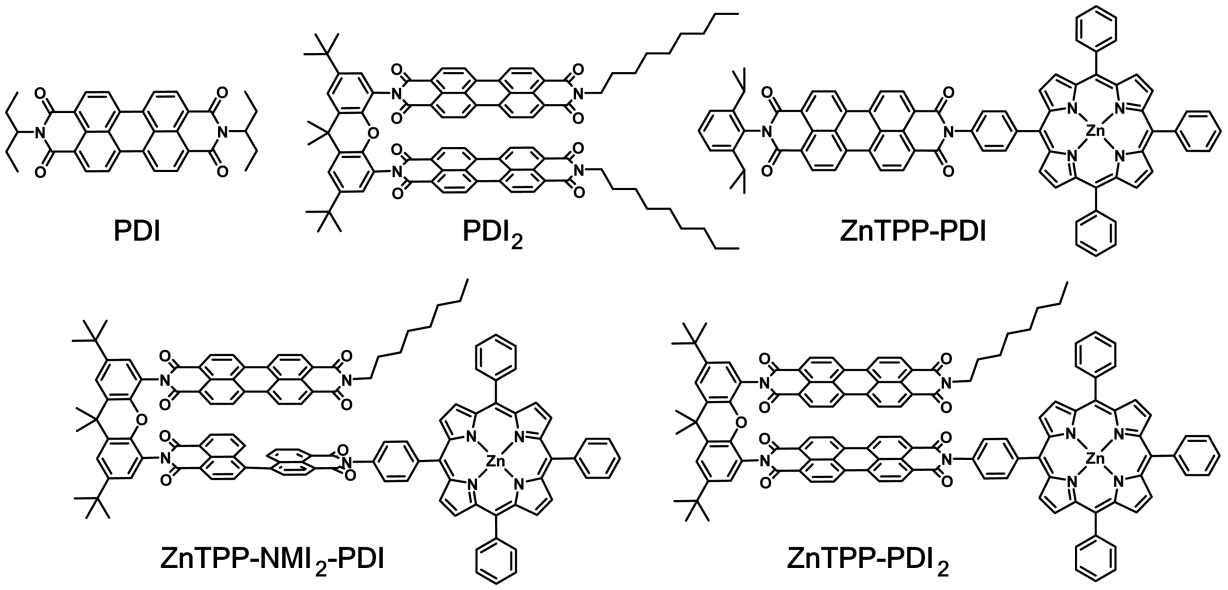

that control PDI aggregation and reduce excimer formation, although crystal engineering of planar PDIs have also been shown to be an effective strategy.[37,38] Increasing the electronic coupling between the PDI units of these molecules through ring-fusion has also led to an increase in efficiency,[39] attributed to increased anion delocalization.[40] Additionally, an increase in anion delocalization across monomeric PDI acceptors in self-segregating π-stacked donor−acceptor oligomers has been shown to reduce geminate recombination rates.[41] These results suggest that the enhancement of charge separation through increased delocalization is not unique to fullerenes and should be an important factor in designing high-performance organic electronic materials.

PDIs are easily modified, enabling precise spatial control of appended electron donors, which has proven crucial in understanding their photophysical properties such as excimer formation[42] and exciton migration.[43] The tendency of PDIs to aggregate has motivated their use in a number of supramolecular charge transfer systems, some of which result in the formation of free carriers.[41,44−49] This relative ease of control makes PDI an ideal model platform for investigating charge transfer dynamics and has led to greatly improved PDI-based photoactive materials.

Here we investigate the influence of anion delocalization on electron transfer using zinc *meso*-tetraphenylporphyrin (ZnTPP) as a donor and a cofacial PDI dimer as the acceptor, ZnTPP-PDI_2 (Scheme 1). The xanthene-bridged PDI dimer was chosen as an electron acceptor to study anion delocalization as it is relatively easy to prepare, and provides a fixed cofacial interaction between the PDI units.[50] Using ZnTPP as a donor allows for minimal overlap of donor and acceptor absorption features for selective excitation and easily identified transient features. The PDI molecules of the dimer are positioned in a cofacial orientation relative to one another by attaching them to the 4- and 5-positions of a xanthene spacer at one imide group of each PDI. At the same time, the distal imide group of one PDI is linked to the *para*-position of one phenyl group in ZnTPP to yield ZnTPP-PDI_2. The data for the dimers is compared to two different porphyrin-PDI monomer reference systems designed to probe electron transfer to each of the individual PDI molecules comprising the PDI_2 unit. In one reference system, one imide of a PDI monomer is attached to the *para*-position of one ZnTPP phenyl group to yield ZnTPP-PDI, thus mimicking the PDI molecule directly bonded to ZnTPP in ZnTPP-PDI_2. In the second reference system, the PDI directly linked to the porphyrin is replaced by a "broken PDI" comprising a bis-4,4′-naphthalene-1,8-dicarboximide dimer, a xanthene spacer, and a PDI to yield ZnTPP-NMI_2-PDI, thus mimicking the second PDI that is not directly attached to the porphyrin in ZnTPP-PDI_2. Importantly, the NMI_2 species cannot be reduced by the lowest excited singlet state of ZnTPP, and thus only through-space electron transfer to the single PDI can occur because of the large number of bonds between it and ZnTPP. The electron transfer rate from the ZnTPP lowest excited singlet state to PDI_2 is increased by 50% versus that in ZnTPP-PDI, when the data are corrected for the statistics of having two electron acceptors. Femtosecond transient IR absorption spectroscopy provides evidence that the observed enhancement in charge separation results from electron transfer producing a delocalized PDI_2 anion.

EXPERIMENTAL SECTION

Synthesis. The synthesis and characterization of each molecule is described in the Supporting Information.

Steady-State Spectroscopy. UV−vis spectra were acquired on a Shimadzu UV-1800 spectrophotometer. FT-IR spectra were measured on a Shimadzu IRAffinity-1 spectrophotometer in transmission mode at 2 cm^{-1} resolution. Samples with a maximum optical density of 1 were prepared in dichloromethane under an N_2 atmosphere, contained in a liquid demountable cell (Harrick Scientific) with CaF_2 windows and a 150 μm Teflon spacer. Chemically reduced samples were prepared by adding molar equivalents of cobaltocene ($CoCp_2$) to solutions of PDI and PDI_2 in dichloromethane, which were then sealed under an N_2 atmosphere in the liquid IR cell.

Computational Details. To reduce computational time, density functional theory (DFT) calculations were performed in TeraChem (version 1.5) at the B3LYP-D3/6-31+G* level of theory for all geometry optimizations. Frequency calculations were performed in Q-Chem (version 4.3) at the B3LYP-D3/6-31G* level of theory with methyl groups placed at the imide positions. A frequency scaling factor of 0.964 was used for all calculated IR frequencies.[51]

DOI: 10.1021/jacs.6b10140
J. Am. Chem. Soc. 2017, 139, 749−756

Transient Absorption Spectroscopy. Femtosecond transient visible and near-infrared (NIR) absorption (fsTA) spectroscopy was performed as described previously.[52] Briefly, the output of a commercial Ti:sapphire oscillator/amplifier (Tsunami/Spitfire, Spectra-Physics) was split with one beam used to generate the 100 fs, 588 nm excitation pulse using a lab-built optical parametric amplifier,[53] and the second to generate a white light probe using either a sapphire crystal for the visible range and a proprietary crystal for the NIR spectral region (Ultrafast Systems, LLC). The overall instrument response was 200 fs. Transient spectra were collected using customized detectors in the visible and NIR spectral regions (Helios, Ultrafast Systems, LLC).

Femtosecond transient IR absorption (fsIR) spectroscopy was performed using a commercial Ti:sapphire oscillator/amplifier (Solstice 3.5W, Spectra-Physics) to pump two optical parametric amplifiers (TOPAS-C, Light Conversion), one which provided a 100 fs, 588 nm excitation pulse and the other provided 100 fs pulses at 1500−1800 cm^{-1}. The overall instrument response was 300 fs. The spectra were acquired with a liquid N_2-cooled dual channel (2 × 64) MCT array detector that is coupled to a Horiba HR320 monochromator as part of a Helios-IR spectrometer (Ultrafast Systems, LLC). Samples with a maximum optical density of 0.1−0.15 were prepared in freshly distilled dioxane contained in a liquid demountable cell (Harrick Scientific) with CaF_2 windows and a 630 μm Teflon spacer.

RESULTS AND DISCUSSION

Steady-State Characterization. The steady state absorption spectra of ZnTPP-PDI, ZnTPP-NMI_2-PDI, and ZnTPP-PDI_2 are shown in Figure 1. The absorption spectrum of ZnTPP-PDI matches that of ZnTPP-NMI_2-PDI with the exception of enhanced UV absorption from NMI in ZnTPP-NMI_2-PDI. This is expected since both molecules have a single ZnTPP donor and a single PDI acceptor. The spectrum of ZnTPP-PDI_2 exhibits a broadening of the PDI absorbance between 450 and 550 nm and enhancement of the band at 490 nm versus that at 530 nm, resulting from interaction between the two PDI transition dipoles as commonly observed in cofacial dimers and explained by exciton coupling models.[42,54−57] The lowest energy porphyrin Q-band absorption occurs at 588 nm in ZnTPP-PDI, and ZnTPP-NMI_2-PDI, and at 590 nm in ZnTPP-PDI_2. The apparent shift in the Q-band absorption is a result of overlap with the broadened PDI absorption in ZnTPP-PDI_2 but the absorption of PDI at this wavelength is minor compared to the ZnTPP donor allowing ZnTPP to be selectively excited at 588 nm.

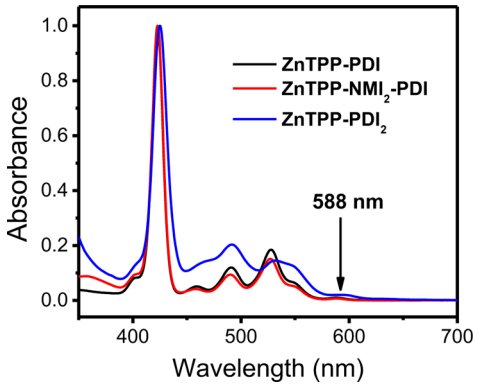

Figure 1. Optical absorption spectra of the indicated compounds in dioxane. The excitation wavelength used for the fsTA and fsIR experiments (588 nm) is marked.

Electrochemistry of the monomeric and dimeric PDI species shows that coupling between the two in ZnTPP-PDI_2 has a minimal effect on reduction potential (Figure S1). Using the Weller formalism (see SI), the free energies for the charge separation reactions: ^{1}*ZnTPP-PDI_n → ZnTPP$^{+\bullet}$-$PDI_n^{-\bullet}$ (n = 1 or 2) are ΔG_{CS} = −0.44 eV and −0.43 eV, respectively, while that of ^{1}*ZnTPP-NMI_2-PDI_n → ZnTPP$^{+\bullet}$-NMI_2-$PDI^{-\bullet}$ is ΔG_{CS} = −0.43 eV. These large negative free energies of reaction should result in rapid charge separation.

Transient Visible Absorption Spectroscopy. Selected fsTA spectra of ZnTPP-PDI, and ZnTPP-PDI_2 in dioxane are shown in Figure 2. In each case, ^{1}*ZnTPP is observed at early times, characterized by a broad positive feature near 460 nm overlaid with the Q-band bleaches. The PDI radical anion has distinctive absorption peaks centered at 700, 790, and 950 nm,[58] and the growth of these features coupled with the growth of the PDI bleach features at 490 and 530 nm indicate that electron transfer from ^{1}*ZnTPP to PDI occurs. It can be clearly seen in the spectra that the absorption bands of $PDI^{-\bullet}$ are sharp in ZnTPP$^{+\bullet}$-$PDI^{-\bullet}$, but are broadened in ZnTPP$^{+\bullet}$-$PDI_2^{-\bullet}$, which has been attributed to anion delocalization over the dimer.[59] The 700 nm band in ZnTPP-PDI_2 shows no significant broadening or sharpening during charge separation suggesting that the anion is delocalized at a rate faster than charge separation. The observed rapid charge separation rates in these compounds are consistent with their negative free energies of reaction. Upon excitation of PDI at 530 nm, both ZnTPP-PDI and ZnTPP-PDI_2 show rapid excitation energy transfer (<1 ps) to ZnTPP followed by charge separation

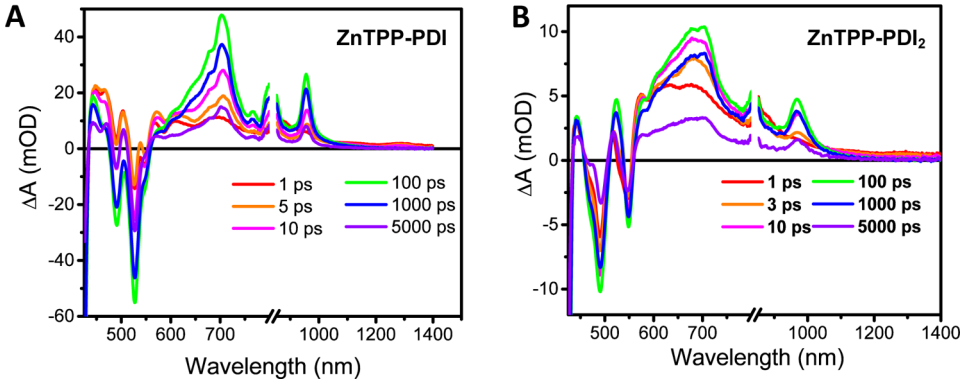

Figure 2. Selected fsTA spectra of (A) ZnTPP-PDI and (B) ZnTPP-PDI_2 excited at 588 nm and probed in the visible and NIR regions.

DOI: 10.1021/jacs.6b10140
J. Am. Chem. Soc. 2017, 139, 749−756

kinetics similar to those observed upon excitation of the ZnTPP Q-band (Figure S5).

The fsTA spectra were globally fit using selected wavelengths according to a first-order model in which charge separation from ^{1}*ZnTPP to yield the radical ion pair is followed by charge recombination to the ground state and to long-lived ^{3}*PDI.[60] Species-associated spectra (SAS) and fits for ZnTPP-PDI, ZnTPP-PDI$_2$, and ZnTPP-NMI$_2$-PDI in dioxane measured in triplicate on independent samples are shown in Figures S2–S4, and the averaged fit parameters with their standard deviations are reported in Table 1. The SAS show the

Table 1. Summary of Electron Transfer Rate Constants Observed by fsTA Spectroscopy[a]

molecule	k_{CS} (s^{-1})	k_{CR} (s^{-1})
ZnTPP-PDI	$8.1 \pm 0.1 \times 10^{10}$	$9.7 \pm 0.1 \times 10^{8}$
ZnTPP-NMI$_2$-PDI	$1.0 \pm 0.1 \times 10^{10}$	$<10^{8}$
ZnTPP-PDI$_2$	$1.4 \pm 0.1 \times 10^{11}$	$7.1 \pm 0.1 \times 10^{8}$

[a]All data listed show the average and standard deviation of three independent samples.

characteristic absorption features of ^{1}*ZnTPP-PDI$_n$ → ZnTPP$^{+\bullet}$-PDI$_n^{-\bullet}$ → ZnTPP-^{3}*PDI$_n$, (n = 1 or 2) and show broadening of the PDI$^{-\bullet}$ absorption bands in the case of the PDI$_2$ acceptor. The expected statistical charge separation rate constant (k_{stat}) for ZnTPP-PDI$_2$ is the sum of the rate constants observed for the ZnTPP-PDI and ZnTPP-NMI$_2$-PDI reference molecules, $k_{stat(ZnTPP\text{-}PDI2)} = k_{CS(ZnTPP\text{-}PDI)} + k_{CS(ZnTPP\text{-}NMI2\text{-}PDI)} = 9.1 \pm 0.2 \times 10^{10}$ s^{-1}. Thus, since $k_{CS(ZnTPP\text{-}PDI2)} = 1.4 \pm 0.1 \times 10^{11}$ s^{-1}, there is a significant ($p < 0.01$) rate enhancement, $k_{CS}/k_{stat} = 1.5 \pm 0.1$ for charge separation to the dimeric PDI structure in ZnTPP-PDI$_2$. A similar effect is not observed for charge recombination where the observed rates for ZnTPP-PDI (9.7×10^8 s^{-1}) and ZnTPP-PDI$_2$ (7.1×10^8 s^{-1}) are similar.

Time-Resolved IR Spectroscopy. Although the fsTA results imply that the anion is delocalized over both PDI subunits in ZnTPP-PDI$_2$, we have also employed fsIR spectroscopy to more closely examine charge delocalization in the reduced acceptor of ZnTPP$^{+\bullet}$-PDI$_2^{-\bullet}$. The contribution to the transient IR absorption spectra from ZnTPP and ZnTPP$^{+\bullet}$ at frequencies >1600 cm^{-1} is negligible as noted by the absence of IR transitions in their steady-state spectra from 1600 to 1800 cm^{-1}.[61,62] In addition, ZnTPP and ZnTPP$^{+\bullet}$ both have comparable IR absorption bands at their C═C stretching frequencies at 1597 cm^{-1}, so that the difference in absorption between these two species at that frequency is small and negligible.[61,62] Thus, we will focus on the IR spectra of the PDI and PDI$_2$ acceptors and their radical anions using the model systems depicted in Scheme 1 because the increased solubility of the model systems allows for decreased IR cell path lengths and smaller solvent artifacts in the steady-state measurements.

Charge sharing on the electron paramagnetic resonance spectroscopy time scale has been reported previously for similar PDI dimers,[50] but this could indicate that the electron is simply hopping on a time scale of 10^7–10^9 s^{-1} between the two PDIs similar to a Robin–Day Class II mixed valence system.[63] If reduction of PDI$_2$ results in a truly delocalized anion, Robin–Day Class III, the transient IR absorption spectra should show that the radical anion is delocalized in PDI$_2^{-\bullet}$ on the IR time scale, as indicated by the fact that the relative vibrational frequency shift of modes affected by the reduction, e.g., the C═O modes between the neutral and reduced species, should be smaller in PDI$_2$ than in the PDI monomer.[63,64]

The ground state IR spectra of the PDI monomer and PDI$_2$ dimer reference molecules (Scheme 1) are shown in Figure 3A along with their calculated spectra. The computed IR spectra agree reasonably well with the experimental spectra after the appropriate scaling factor of 0.964 is applied.[51] The calculated spectra are used to assign the bands in the PDI monomer spectrum at 1694 and 1656 cm^{-1} to C═O stretching modes, and the 1596 cm^{-1} band to a C═C core stretch. In PDI$_2$, the C═O bands broaden and shift to higher frequency at 1706 and 1666 cm^{-1}, and show Davydov splittings of 14 and 17 cm^{-1}, respectively, which leads to pairs of bands at 1713 and 1699 cm^{-1}, as well as 1675 and 1658 cm^{-1}, which is unsurprising considering the sensitivity of these modes to their electronic environment.[65] The PDI$_2$ C═C core stretching mode frequency is unchanged from that of the monomer at 1596 cm^{-1}. The IR spectrum of PDI$^{-\bullet}$ in Figure 3B shows that the C═O stretching bands shift to lower frequencies at 1640 and 1607 cm^{-1}, while the C═C stretch shifts to 1584 cm^{-1}. The corresponding IR spectrum of PDI$_2^{-\bullet}$ shows that the C═O bands in the dimer broaden and downshift to give maxima at 1688 and 1660 cm^{-1} with the Davydov splittings being unresolved, while the C═C stretch shifts slightly to 1592 cm^{-1}. The spectral shifts of the C═O stretches in PDI$_2^{-\bullet}$ relative to those of PDI$_2$ are only 25 and 39 cm^{-1}, while of those of PDI$^{-\bullet}$ relative to PDI are 54 and 49 cm^{-1}. These results and the coalescence of the IR bands in PDI$_2^{-\bullet}$ suggest that the charge is substantially shared between the two PDI molecules on a time

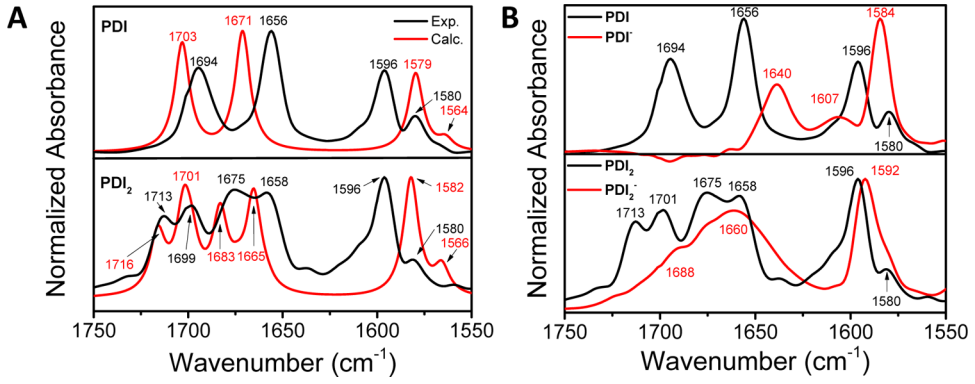

Figure 3. (A) Comparisons between the measured IR spectra of PDI and PDI$_2$ in CH_2Cl_2, and their calculated spectra (B3LYP-d3, 6-31+G*). (B) Comparisons between the IR spectra of PDI and PDI$_2$ and their respective anions, PDI$^{-\bullet}$ and PDI$_2^{-\bullet}$, in CH_2Cl_2.

DOI: 10.1021/jacs.6b10140
J. Am. Chem. Soc. 2017, 139, 749–756

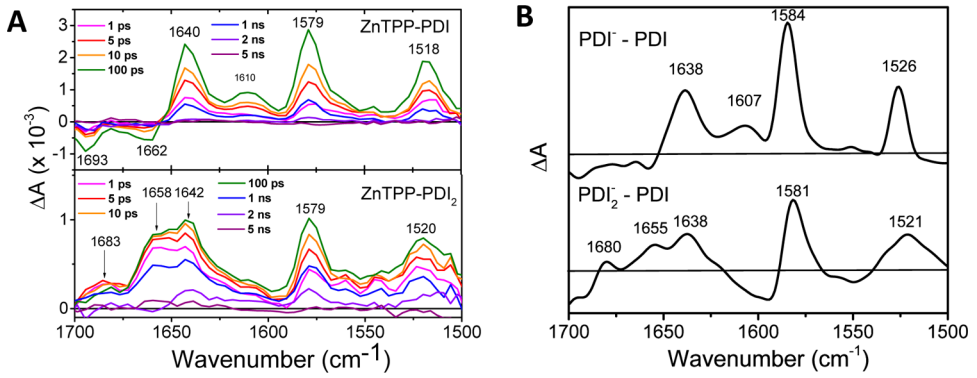

Figure 4. (A) FsIR spectra for ZnTPP-PDI and ZnTPP-PDI_2 at the indicated times following a 120 fs, 588 nm laser pulse. (B) Simulated transient IR absorption spectra for the reduction of PDI and PDI_2 based on their ground state and radical anion spectra in (B).

scale <10 ps as implied by the ~10−30 cm^{-1} difference between the C═O frequencies of $PDI^{-\bullet}$ and $PDI_2^{-\bullet}$.[66,67]

The fsIR spectra of ZnTPP-PDI and ZnTPP-PDI_2 at selected times are shown in Figure 4A, while the global kinetic fits to the data are given in Figure S6, and are in good agreement with the kinetics obtained from fsTA spectroscopy. Using the data in Figure 3B, the scaled IR absorption spectra of PDI, PDI_2, $PDI^{-\bullet}$ and $PDI_2^{-\bullet}$ are used to predict ΔA($PDI^{-\bullet}$-PDI) and ΔA($PDI_2^{-\bullet}$-PDI), Figure 4B. The formation of $ZnTPP^{+\bullet}$-$PDI^{-\bullet}$ is accompanied by the appearance of 1641 and 1610 cm^{-1} C═O absorptions assigned to $PDI^{-\bullet}$ in good agreement with the predicted ΔA($PDI^{-\bullet}$-PDI) transient absorption spectrum in Figure 4B. In addition, the 1596 cm^{-1} C═C stretching mode in PDI downshifts to 1579 cm^{-1} in $ZnTPP^{+\bullet}$-$PDI^{-\bullet}$. The observed transient IR absorption spectra for $ZnTPP^{+\bullet}$-$PDI_2^{-\bullet}$ (Figure 4A) show broad C═O absorptions at 1683, 1658, and 1642 cm^{-1} and a C═C stretch at 1579 cm^{-1}, which also agree well with the predicted ΔA($PDI_2^{-\bullet}$-PDI) spectrum shown in Figure 4B. These changes in frequency result from placing an electron in the PDI LUMO, which weakens the π-bonds in PDI. The C═O stretching frequencies are particularly sensitive to the electron density in the PDI LUMO because the charge density is higher on the more electronegative oxygen atoms. Sharing the charge between the two PDI molecules in $ZnTPP^{+\bullet}$-$PDI_2^{-\bullet}$ results in less weakening the C═O π-bonds in each PDI of the dimer, which reduces the shifts to lower frequency relative to those of monomeric $PDI^{-\bullet}$. The spectra of $ZnTPP^{+\bullet}$-$PDI_2^{-\bullet}$ exhibit a slight increase in ΔA at 1642 cm^{-1} relative to 1658 cm^{-1} as charge separation proceeds, which may be due to intramolecular vibrational relaxation, but at no time following photoexcitation do the spectra resemble those of $ZnTPP^{+\bullet}$-$PDI^{-\bullet}$. This behavior is consistent with a strong electronic interaction between the two PDIs in $ZnTPP^{+\bullet}$-$PDI_2^{-\bullet}$ being maintained during the course of charge separation, and also implies that anion delocalization is faster than charge separation in ZnTPP-PDI_2.

Anion Delocalization and Electron Transfer. Recent experimental and theoretical studies have invoked charge delocalization to explain the unexpectedly high yield of free charge carriers in BHJ OPVs.[8,9,21,27,29] Liu and Troisi have focused on the role of low-lying anion excited states that can reduce the effective ΔG_{CS} for charge separation in the inverted region of the Marcus rate vs free energy profile leading to an increased charge separation rate.[68] Higher level calculations have been used to predict a lower reorganization energy for hole transfer in DNA when the hole is able to delocalize over multiple bases.[69,70] In addition, the experimental observation of a low reorganization energy, and thus efficient hole transport in pentacene has been attributed to charge delocalization.[71] We have also observed enhanced charge transfer rates in supramolecular donor−acceptor systems in which delocalization is possible.[45,47] However, Savoie et al.[8] and Jakowetz et al.[29] have recently pointed out that the Marcus picture of nonadiabatic electron transfer may be inappropriate for polymer−fullerene blends in the solid state, where a high density of charge transfer states that are accessed by the excited state of the donor and extensive charge delocalization may promote rapid charge separation and subsequent transport.

Nevertheless, for small molecules in solution, such as ZnTPP-PDI and ZnTPP-PDI_2, which undergo nonadiabatic electron transfer in the weak coupling regime, Marcus electron transfer theory is usually an effective model, which describes the reaction rate in terms of the electronic coupling matrix element, V, and the Franck−Condon-weighted density of states that depends on the ΔG of reaction and the total nuclear reorganization energy, λ, for the process.[72,73]

The value of λ comprises both a solvent contribution, λ_S and a contribution from the internal vibrational modes of the reactants and products, λ_I. Marcus employed dielectric continuum theory to predict the dependence of λ_S on the ionic radii and the distance between the ions[72,73]

$$\lambda_S = e^2\left(\frac{1}{2r_D} + \frac{1}{2r_A} - \frac{1}{r_{DA}}\right)\left(\frac{1}{\varepsilon_{op}} - \frac{1}{\varepsilon_S}\right) \quad (1)$$

where e is the charge of an electron, r_D and r_A are the ionic radii of the donor and acceptor, respectively, r_{DA} is the donor−acceptor center-to-center distance, ε_{op} is the high frequency dielectric constant of the solvent (usually approximated by $\varepsilon_{op} = n^2$, where n is the solvent refractive index), and ε_S is the dielectric constant of the solvent. Using eq 1 and the values of these parameters given in the SI yields $\lambda_S = 0.06 \pm 0.01$ eV for both ZnTPP-PDI and ZnTPP-PDI_2 in dioxane, so that charge delocalization has a negligible effect on λ_S. Given the well-recognized limitations of the dielectric continuum solvation model,[74] it is not useful to base a rate argument on very small differences in λ_S. Using DFT, we find that $\lambda_I = 0.13 \pm 0.01$ eV for both PDI and PDI_2; thus the total λ is essentially unchanged for reduction of PDI and PDI_2 (see SI). Although charge delocalization in $PDI_2^{-\bullet}$ should result in a significant increase in the number of vibrational modes that contribute to λ_I relative to $PDI^{-\bullet}$, this increase is offset by the smaller frequency change that occurs when a partial charge resides on each PDI within

DOI: 10.1021/jacs.6b10140
J. Am. Chem. Soc. 2017, 139, 749−756

$PDI_2^{-\bullet}$, resulting in no appreciable change in λ_I for $PDI^{-\bullet}$ versus $PDI_2^{-\bullet}$.

Given that ΔG_{CS} is also approximately the same for ZnTPP-PDI and ZnTPP-PDI_2, it is likely that the increase in charge separation rate for ZnTPP-PDI_2 relative to ZnTPP-PDI is a consequence of an increase in electronic coupling. The DFT-optimized structures for $PDI_2^{-\bullet}$ have electron density residing on both PDIs in the SOMO and SOMO+1 (Figure S8). Moreover, these calculations show that the SOMO+1 energies of $PDI^{-\bullet}$ and $PDI_2^{-\bullet}$ are 2.38 and 0.88 eV, respectively, above their corresponding SOMO energies. Given that $ZnTPP^{+\bullet}$-$PDI^{-\bullet}$ and $ZnTPP^{+\bullet}$-$PDI_2^{-\bullet}$ are nearly isoenergetic, this places the SOMO+1 energies of the PDI and $PDI_2^{-\bullet}$ acceptors approximately 1.94 and 0.45 eV, respectively, above that of ^{1}*ZnTPP. Thus, a superexchange interaction that mixes ^{1}*ZnTPP (A) with the states described largely by the SOMO +1 (B) and SOMO (C) of the PDI acceptors will result in an electronic coupling $V = V_{AB} \cdot V_{BC}/\Delta E_{AB}$,[75] where ΔE_{AB} is the energy gap between ^{1}*ZnTPP and the state involving the acceptor SOMO+1 (1.94 eV for $PDI^{-\bullet}$ 0.45 eV for $PDI_2^{-\bullet}$ as noted above). Since the charge separation rate constant $k_{CS} \propto V^2$, the rate ratio for charge separation to the acceptors will be given by eq 2:

$$\frac{k_{CS}(PDI_2)}{k_{CS}(PDI)} = \left(\frac{V_{AB}(PDI_2)}{V_{AB}(PDI)} \cdot \frac{V_{BC}(PDI_2)}{V_{BC}(PDI)} \cdot \frac{\Delta E_{AB}(PDI)}{\Delta E_{AB}(PDI_2)} \right)^2 \quad (2)$$

A rough approximation of the ratio $V_{AB}(PDI_2)/V_{AB}(PDI)$ can be made using the spin densities at the nitrogen atoms that join PDI to the phenyl groups of ZnTPP in ZnTPP-PDI_2 (−0.00558) and ZnTPP-PDI (−0.01251), while we assume to a first approximation that $V_{BC}(PDI_2)/V_{BC}(PDI) \cong 1$, because the ratios of the orbital coefficients for the SOMO and SOMO +1 in $PDI^{-\bullet}$ and $PDI_2^{-\bullet}$ are similar, so that eq 2 yields $k_{CS}(PDI_2)/k_{CS}(PDI) \cong 4$, which is in line with the modest increase observed experimentally. This also explains why there is no significant change in charge recombination rate since in the charge recombination process an electron is transferred to a single localized $ZnTPP^{+\bullet}$ orbital in both cases.

This analysis shows that charge delocalization within $PDI_2^{-\bullet}$ reduces the energy gap between its SOMO and SOMO+1 as well as between ^{1}*ZnTPP and the SOMO+1 to a sufficient extent that superexchange increases the electron transfer rate to PDI_2. The important point is that the rate increase requires charge transfer directly to a delocalized orbital on PDI_2. A comparison of the fsIR spectra of $ZnTPP^{+\bullet}$-$PDI^{-\bullet}$ and $ZnTPP^{+\bullet}$-$PDI_2^{-\bullet}$ show that the anion is delocalized in the latter on the vibrational time scale, which is consistent with this picture. In a fully delocalized oligomeric acceptor, $A_n^{-\bullet}$, increasing the number of delocalized states, SOMO+1, SOMO+2, etc., will decrease the energy gaps between these states and the donor excited state ^{1}*D resulting in a stronger superexchange interaction that increases the charge separation rate. However, the superexchange model breaks down in the limit where the density of states is high enough to form a band that has a sufficient energy range so that there are acceptor states at or below the energy of ^{1}*D.[75] This situation seems likely in the solid state, where charge injection directly to accessible states of the acceptor aggregates enhances the rates.[8,29] As the density of acceptor states increases, a band structure model may be required to best describe the electronic structure of the acceptor, as has been discussed for fullerenes in BHJ OPVs.[8] Similar arguments can be made if an initially photoexcited acceptor ^{1}*A carries out hole transfer to produce delocalized donor states, $D^{+\bullet}$.[28]

CONCLUSIONS

Photoinduced charge separation in ZnTPP-PDI_2 is about 50% faster than in ZnTPP-PDI, when the data are corrected for the statistics of having two electron acceptors. Femtosecond transient IR absorption spectroscopy provides evidence that the observed enhancement in charge separation results from electron transfer to a delocalized PDI_2 anion. An analysis of the energetics of charge separation shows that both ΔG_{CS} and λ for charge separation are very similar in both molecules, which points toward a difference in electronic coupling being responsible for the observed difference. DFT calculations show that the energy gap between the SOMO and SOMO+1 in the reduced acceptors is significantly smaller for $PDI_2^{-\bullet}$ relative to $PDI^{-\bullet}$, and that the charge is fully delocalized over both PDI molecules in both the SOMO and SOMO+1 of $PDI_2^{-\bullet}$. This makes it possible that more effective mixing of the $PDI_2^{-\bullet}$ electronic state involving its SOMO+1 with ^{1}*ZnTPP in a superexchange interaction can account for the modest increase in the charge separation rate in ZnTPP-PDI_2 relative to ZnTPP-PDI. This mechanism requires that the electron transferred from ^{1}*ZnTPP directly populates the delocalized $PDI_2^{-\bullet}$ state. This result is significant because charge transfer directly to delocalized states has been shown to be important for BHJ OPV performance efficiency. Being able to take advantage of a superexchange interaction with low-lying states afforded by delocalization suggests that the availability of these delocalized states could be used as a design criterion for ultrafast charge carrier generation to enhance performance in OPVs using small molecule donor−acceptor systems. An interesting remaining theoretical and experimental question is at what aggregate size do the energetics and couplings between individual molecules within a small ordered oligomeric array transition from superexchange mediated charge separation to direct electron transfer involving energetically accessible states of the oligomeric acceptor. We are working toward answering this question in a series of structurally well-defined donor−oligomeric acceptor structures.

ASSOCIATED CONTENT

Supporting Information

The Supporting Information is available free of charge on the ACS Publications website at DOI: 10.1021/jacs.6b10140.

Additional information describing synthesis and electrochemistry, as well as additional fsTA data (PDF)

AUTHOR INFORMATION

Corresponding Authors

*t-marks@northwestern.edu

*m-wasielewski@northwestern.edu

ORCID

Tobin J. Marks: 0000-0001-8771-0141

Michael R. Wasielewski: 0000-0003-2920-5440

Notes

The authors declare no competing financial interest.

DOI: 10.1021/jacs.6b10140
J. Am. Chem. Soc. 2017, 139, 749−756

■ ACKNOWLEDGMENTS

This work was supported by the Argonne-Northwestern Solar Energy Research (ANSER) Center, an Energy Frontier Research Center funded by the U.S. Department of Energy (DOE), Office of Science, Office of Basic Energy Sciences, under award number DE-SC0001059. C.M.M. was supported by a NSF Graduate Research Fellowship under grant no. DGE-1324585.

■ REFERENCES

(1) Wasielewski, M. R. *Chem. Rev.* **1992**, *92*, 435.
(2) Gust, D.; Moore, T. A.; Moore, A. L. *Acc. Chem. Res.* **2001**, *34*, 40.
(3) Wasielewski, M. R. *Acc. Chem. Res.* **2009**, *42*, 1910.
(4) Gust, D.; Moore, T. A.; Moore, A. L. *Acc. Chem. Res.* **2009**, *42*, 1890.
(5) Rudolf, M.; Kirner, S. V.; Guldi, D. M. *Chem. Soc. Rev.* **2016**, *45*, 612.
(6) Segura, J. L.; Martin, N.; Guldi, D. M. *Chem. Soc. Rev.* **2005**, *34*, 31.
(7) Heitzer, H. M.; Savoie, B. M.; Marks, T. J.; Ratner, M. A. *Angew. Chem., Int. Ed.* **2014**, *53*, 7456.
(8) Savoie, B. M.; Rao, A.; Bakulin, A. A.; Gelinas, S.; Movaghar, B.; Friend, R. H.; Marks, T. J.; Ratner, M. A. *J. Am. Chem. Soc.* **2014**, *136*, 2876.
(9) Bakulin, A. A.; Rao, A.; Pavelyev, V. G.; van Loosdrecht, P. H. M.; Pshenichnikov, M. S.; Niedzialek, D.; Cornil, J.; Beljonne, D.; Friend, R. H. *Science* **2012**, *335*, 1340.
(10) Hestand, N. J.; Kazantsev, R. V.; Weingarten, A. S.; Palmer, L. C.; Stupp, S. I.; Spano, F. C. *J. Am. Chem. Soc.* **2016**, *138*, 11762.
(11) Chenu, A.; Scholes, G. D. *Annu. Rev. Phys. Chem.* **2015**, *66*, 69.
(12) Fuller, F. D.; Pan, J.; Gelzinis, A.; Butkus, V.; Senlik, S. S.; Wilcox, D. E.; Yocum, C. F.; Valkunas, L.; Abramavicius, D.; Ogilvie, J. P. *Nat. Chem.* **2014**, *6*, 706.
(13) Lewis, K. L. M.; Ogilvie, J. P. *J. Phys. Chem. Lett.* **2012**, *3*, 503.
(14) Kitamoto, K.; Sakai, K. *Chem. Commun. (Cambridge, U. K.)* **2016**, *52*, 1385.
(15) Kitamoto, K.; Ogawa, M.; Ajayakumar, G.; Masaoka, S.; Kraatz, H.-B.; Sakai, K. *Inorg. Chem. Front.* **2016**, *3*, 671.
(16) Sariciftci, N. S.; Smilowitz, L.; Heeger, A. J.; Wudl, F. *Science* **1992**, *258*, 1474.
(17) Grancini, G.; Maiuri, M.; Fazzi, D.; Petrozza, A.; Egelhaaf, H. J.; Brida, D.; Cerullo, G.; Lanzani, G. *Nat. Mater.* **2013**, *12*, 29.
(18) Falke, S. M.; Rozzi, C. A.; Brida, D.; Maiuri, M.; Amato, M.; Sommer, E.; De Sio, A.; Rubio, A.; Cerullo, G.; Molinari, E. *Science* **2014**, *344*, 1001.
(19) Hwang, I. W.; Soci, C.; Moses, D.; Zhu, Z.; Waller, D.; Gaudiana, R.; Brabec, C. J.; Heeger, A. J. *Adv. Mater.* **2007**, *19*, 2307.
(20) Forrest, S. R. *MRS Bull.* **2005**, *30*, 28.
(21) Gélinas, S.; Rao, A.; Kumar, A.; Smith, S. L.; Chin, A. W.; Clark, J.; van der Poll, T. S.; Bazan, G. C.; Friend, R. H. *Science* **2014**, *343*, 512.
(22) Onsager, L. *Phys. Rev.* **1938**, *54*, 554.
(23) Braun, C. L. *J. Chem. Phys.* **1984**, *80*, 4157.
(24) Dimitrov, S. D.; Bakulin, A. A.; Nielsen, C. B.; Schroeder, B. C.; Du, J.; Bronstein, H.; McCulloch, I.; Friend, R. H.; Durrant, J. R. *J. Am. Chem. Soc.* **2012**, *134*, 18189.
(25) Tamura, H.; Burghardt, I. *J. Am. Chem. Soc.* **2013**, *135*, 16364.
(26) Jailaubekov, A. E.; Willard, A. P.; Tritsch, J. R.; Chan, W.-L.; Sai, N.; Gearba, R.; Kaake, L. G.; Williams, K. J.; Leung, K.; Rossky, P. J. *Nat. Mater.* **2013**, *12*, 66.
(27) D'Avino, G.; Muccioli, L.; Olivier, Y.; Beljonne, D. *J. Phys. Chem. Lett.* **2016**, *7*, 536.
(28) Feier, H. M.; Reid, O. G.; Pace, N. A.; Park, J.; Bergkamp, J. J.; Sellinger, A.; Gust, D.; Rumbles, G. *Adv. Energy Mater.* **2016**, *6*, 1502176.
(29) Jakowetz, A. C.; Böhm, M. L.; Zhang, J.; Sadhanala, A.; Huettner, S.; Bakulin, A. A.; Rao, A.; Friend, R. H. *J. Am. Chem. Soc.* **2016**, *138*, 11672.
(30) Gregg, B. A. *J. Phys. Chem. Lett.* **2011**, *2*, 3013.
(31) Pensack, R. D.; Guo, C.; Vakhshouri, K.; Gomez, E. D.; Asbury, J. B. *J. Phys. Chem. C* **2012**, *116*, 4824.
(32) Jackson, N. E.; Savoie, B. M.; Chen, L. X.; Ratner, M. A. *J. Phys. Chem. Lett.* **2015**, *6*, 1018.
(33) Chen, J. D.; Cui, C.; Li, Y. Q.; Zhou, L.; Ou, Q. D.; Li, C.; Li, Y.; Tang, J. X. *Adv. Mater.* **2015**, *27*, 1035.
(34) He, Z.; Xiao, B.; Liu, F.; Wu, H.; Yang, Y.; Xiao, S.; Wang, C.; Russell, T. P.; Cao, Y. *Nat. Photonics* **2015**, *9*, 174.
(35) Guo, X.; Zhou, N.; Lou, S. J.; Smith, J.; Tice, D. B.; Hennek, J. W.; Ortiz, R. P.; Navarrete, J. T. L.; Li, S.; Strzalka, J. *Nat. Photonics* **2013**, *7*, 825.
(36) Meng, D.; Fu, H.; Xiao, C.; Meng, X.; Winands, T.; Ma, W.; Wei, W.; Fan, B.; Huo, L.; Doltsinis, N. L.; Li, Y.; Sun, Y.; Wang, Z. *J. Am. Chem. Soc.* **2016**, *138*, 10184.
(37) Hartnett, P. E.; Margulies, E. A.; Mauck, C. M.; Miller, S. A.; Wu, Y.; Wu, Y.-L.; Marks, T. J.; Wasielewski, M. R. *J. Phys. Chem. B* **2016**, *120*, 1357.
(38) Hartnett, P. E.; Timalsina, A.; Matte, H. S. S. R.; Zhou, N.; Guo, X.; Zhao, W.; Facchetti, A.; Chang, R. P. H.; Hersam, M. C.; Marks, T. J.; Wasielewski, M. R. *J. Am. Chem. Soc.* **2014**, *136*, 16345.
(39) Zhong, H.; Wu, C. H.; Li, C. Z.; Carpenter, J.; Chueh, C. C.; Chen, J. Y.; Ade, H.; Jen, A. K. Y. *Adv. Mater.* **2016**, *28*, 951.
(40) Hartnett, P. E.; Matte, H. S. S. R.; Eastham, N. D.; Jackson, N. E.; Wu, Y.; Chen, L. X.; Ratner, M. A.; Chang, R. P. H.; Hersam, M. C.; Marks, T. J.; Wasielewski, M. R. *Chem. Sci.* **2016**, *7*, 3543.
(41) Roznyatovskiy, V. V.; Carmieli, R.; Dyar, S. M.; Brown, K. E.; Wasielewski, M. R. *Angew. Chem., Int. Ed.* **2014**, *53*, 3457.
(42) Margulies, E. A.; Shoer, L. E.; Eaton, S. W.; Wasielewski, M. R. *Phys. Chem. Chem. Phys.* **2014**, *16*, 23735.
(43) Marciniak, H.; Li, X.-Q.; Würthner, F.; Lochbrunner, S. *J. Phys. Chem. A* **2010**, *115*, 648.
(44) Bu, L.; Guo, X.; Yu, B.; Qu, Y.; Xie, Z.; Yan, D.; Geng, Y.; Wang, F. *J. Am. Chem. Soc.* **2009**, *131*, 13242.
(45) Bullock, J. E.; Carmieli, R.; Mickley, S. M.; Vura-Weis, J.; Wasielewski, M. R. *J. Am. Chem. Soc.* **2009**, *131*, 11919.
(46) Guzman, C. X.; Calderon, R. M. K.; Li, Z.; Yamazaki, S.; Peurifoy, S. R.; Guo, C.; Davidowski, S. K.; Mazza, M. M. A.; Han, X.; Holland, G. *J. Phys. Chem. C* **2015**, *119*, 19584.
(47) Hartnett, P. E.; Dyar, S. M.; Margulies, E. A.; Shoer, L. E.; Cook, A. W.; Eaton, S. W.; Marks, T. J.; Wasielewski, M. R. *Chem. Sci.* **2015**, *6*, 402.
(48) Ley, D.; Guzman, C. X.; Adolfsson, K. H.; Scott, A. M.; Braunschweig, A. B. *J. Am. Chem. Soc.* **2014**, *136*, 7809.
(49) Li, W. S.; Saeki, A.; Yamamoto, Y.; Fukushima, T.; Seki, S.; Ishii, N.; Kato, K.; Takata, M.; Aida, T. *Chem. - Asian J.* **2010**, *5*, 1566.
(50) Tauber, M. J.; Kelley, R. F.; Giaimo, J. M.; Rybtchinski, B.; Wasielewski, M. R. *J. Am. Chem. Soc.* **2006**, *128*, 1782.
(51) Merrick, J. P.; Moran, D.; Radom, L. *J. Phys. Chem. A* **2007**, *111*, 11683.
(52) Young, R. M.; Dyar, S. M.; Barnes, J. C.; Juríček, M.; Stoddart, J. F.; Co, D. T.; Wasielewski, M. R. *J. Phys. Chem. A* **2013**, *117*, 12438.
(53) Greenfield, S. R.; Wasielewski, M. R. *Opt. Lett.* **1995**, *20*, 1394.
(54) Giaimo, J. M.; Lockard, J. V.; Sinks, L. E.; Scott, A. M.; Wilson, T. M.; Wasielewski, M. R. *J. Phys. Chem. A* **2008**, *112*, 2322.
(55) Son, M.; Park, K. H.; Shao, C.; Würthner, F.; Kim, D. *J. Phys. Chem. Lett.* **2014**, *5*, 3601.
(56) Kasha, M.; Rawls, H. R.; Ashraf El-Bayoumi, M. *Pure Appl. Chem.* **1965**, *11*, 371.
(57) Spano, F. C. *Acc. Chem. Res.* **2009**, *43*, 429.
(58) Gosztola, D.; Niemczyk, M. P.; Svec, W.; Lukas, A. S.; Wasielewski, M. R. *J. Phys. Chem. A* **2000**, *104*, 6545.
(59) van der Boom, T.; Hayes, R. T.; Zhao, Y.; Bushard, P. J.; Weiss, E. A.; Wasielewski, M. R. *J. Am. Chem. Soc.* **2002**, *124*, 9582.
(60) Ford, W. E.; Kamat, P. V. *J. Phys. Chem.* **1987**, *91*, 6373.
(61) Andersson, L. A.; Loehr, T. M.; Thompson, R. G.; Strauss, S. H. *Inorg. Chem.* **1990**, *29*, 2142.
(62) Gross, Z.; Barzilay, C. *Angew. Chem., Int. Ed. Engl.* **1992**, *31*, 1615.

DOI: 10.1021/jacs.6b10140
J. Am. Chem. Soc. 2017, 139, 749−756

(63) Atwood, C. G.; Geiger, W. E. *J. Am. Chem. Soc.* **2000**, *122*, 5477.
(64) Robin, M. B.; Day, P. *Adv. Inorg. Chem. Radiochem.* **1967**, *10*, 247.
(65) Pensack, R. D.; Banyas, K. M.; Asbury, J. B. *Phys. Chem. Chem. Phys.* **2010**, *12*, 14144.
(66) Kubiak, C. P. *Inorg. Chem.* **2013**, *52*, 5663.
(67) Zoerb, M. C.; Henderson, J. S.; Glover, S. D.; Lomont, J. P.; Nguyen, S. C.; Hill, A. D.; Kubiak, C. P.; Harris, C. B. *J. Phys. Chem. B* **2015**, *119*, 10738.
(68) Liu, T.; Troisi, A. *Adv. Mater.* **2013**, *25*, 1038.
(69) LeBard, D. N.; Lilichenko, M.; Matyushov, D. V.; Berlin, Y. A.; Ratner, M. A. *J. Phys. Chem. B* **2003**, *107*, 14509.
(70) Siriwong, K.; Voityuk, A. A.; Newton, M. D.; Rösch, N. *J. Phys. Chem. B* **2003**, *107*, 2595.
(71) Gruhn, N. E.; da Silva Filho, D. A.; Bill, T. G.; Malagoli, M.; Coropceanu, V.; Kahn, A.; Brédas, J.-L. *J. Am. Chem. Soc.* **2002**, *124*, 7918.
(72) Marcus, R. A. *J. Chem. Phys.* **1956**, *24*, 966.
(73) Marcus, R. A. *J. Chem. Phys.* **1965**, *43*, 679.
(74) Newton, M. D. *Adv. Chem. Phys.* **1999**, *106*, 303.
(75) Plato, M.; Möbius, K.; Michel-Beyerle, M. E.; Bixon, M.; Jortner, J. *J. Am. Chem. Soc.* **1988**, *110*, 7279.

DOI: 10.1021/jacs.6b10140
J. Am. Chem. Soc. 2017, 139, 749−756